ELSEVIER

Wear 203–204 (1997) 98–106

WEAR

Wear of high-velocity oxy-fuel (HVOF)-coated cones in rolling contact

R. Ahmed, M. Hadfield

Brunel University, Department of Mechanical Engineering, Uxbridge UB8 3PH, UK

Abstract

An experimental approach using a modified four-ball machine was used to investigate the rolling-contact fatigue (RCF) performance of tungsten carbide cobalt (WC-12%Co) coatings deposited by the high-velocity oxy-fuel (HVOF) process. The coated rolling-elements were in the geometrical shape of a cone which replaced the upper ball of the modified four-ball machine. The RCF tests simulate the configuration of a deep groove rolling-element ball bearing, and the tests were conducted in a conventional steel ball bearing and hybrid ceramic bearing configurations. The coating thickness, Hertz contact stress and the test lubricants were varied to provide various tribological conditions during the tests. Three different coating thicknesses were investigated and the coatings were ground and polished to attain a good surface finish on the rolling elements. The effect of substrate hardness, coating thickness and fluid film thickness on the RCF performance have been investigated along with the coating failure modes. Coating wear has been analysed using a scanning electron microscope (SEM) and the results discussed with the aid of the coating microstructure, microhardness and talysurf analysis of the wear track. Test results reveal that the performance of the coating is dependent upon the combination of the substrate and the coating properties. Moreover, the coating failure is a function of surface and subsurface mechanisms depending upon the tribological conditions during the test. Thinner coatings did not fail at the interface, indicating a good adhesive strength between the coating and the substrate. The depth of the failure and its comparison with the orthogonal shear-stress depth has been discussed. The coating failure was observed to be a combination of surface wear and subsurface delamination.

Keywords: Thermal spraying; HVOF; Rolling-contact fatigue

1. Introduction

Thermally sprayed tungsten carbide cobalt (WC-Co) coatings deposited by high-velocity thermal spraying processes are well known for their resistance against sliding wear, hammer wear, abrasion wear and fretting [1]. This coating process uses higher velocities of the impact particles (typically 750 m s^{-1}) in comparison to the plasma spraying process, which results in a dense and compact coating microstructure. These coatings have shown improvements in the lifetime of components working in hostile environments with corrosion and abrasion [2], etc. These characteristics have enabled thermal spray coatings to become an integral part of the aircraft and automobile industry [3]. The spectrum of applications of these coatings is not limited to tribological problems, but a diversified range of applications such as clearance controls, thermal barriers, marine engineering, etc., are common to the industry. However, the performance of these coatings is application dependent. That is, it depends not only on the service conditions, but also on the coating and the substrate material, coating process parameters, coating thickness and functional grading, etc. In general, it is the combination of the coating and the substrate properties which govern the performance of the coated components. The brittleness and weakness of these coatings due to their lamellar structure have limited these coatings to low-stress applications. The wear behaviour of these coatings thus relies upon the prevailing tribological conditions during a sliding, rolling or rolling/sliding contact. The failure mechanism and wear properties of these coatings can thus vary for different contact conditions. Unfortunately, there is a lack of data available on the performance of these coatings under rolling or rolling/sliding contact. This study addresses one such investigation in which the wear of thermally sprayed WC-Co coatings was investigated in rolling contact under various tribological conditions of lubrication and contact configuration for different coating thicknesses. The lubricants were varied to provide fully developed ($\lambda > 3$), mixed ($\lambda > 1$) and boundary regimes ($\lambda < 1$) (λ = ratio of fluid film thickness to average surface roughness).

During this study a modified four-ball machine, which differs from the four-ball machine in the sense that the lower planetary balls are free to rotate, was used to investigate the rolling-contact fatigue (RCF) performance of thermal spray coatings. The failed rolling-element coatings are analysed for surface failures using scanning electron microscope (SEM)

PII S0043-1648(96)07349-8

observations. The results are discussed with the help of microhardness measurements, coating microstructure and talysurf analysis of the wear track.

1.1. Previous RCF studies

Initial studies on the RCF behaviour of thermally sprayed ceramic and metallic coatings were reported by Tobe et al. [4] using a two-roller type rolling-fatigue test machine. They observed that the surface roughness of the rollers was significant to the fatigue performance, and a roller design to support the coatings at the edges can improve the fatigue life. Later studies by Tobe et al. [5] on an aluminium substrate revealed that the compressive strength of the coating and the shear stress between the coating and the substrate are the most important factors for the RCF performance of these coatings. The test results showed that the variation in tribological conditions can alter the failure mechanism of these coatings; moreover, significant residual stresses can be generated within the coating microstructure during the RCF tests.

Makela et al. [6], during their experimental approach to study the RCF behaviour of WC-12%Co coated steel rollers using a three-roller and two-roller type test machine, revealed that the behaviour of these coatings not only depend upon Hertz contact stress, but also on the tribological conditions and vibration during the test. Similarly, Sahoo [7] studied the RCF resistance of WC-Co coatings in the slat and flap track of the aircraft wing under high stresses, and reported that cracks initiated from the surface and progressed through the coating thickness. Hadfield et al. [8] during their study of D-gun coatings reported that the WC-Co coatings failed within the coating microstructure, whereas the Al_2O_3 coatings failed at the interface. Yoshida et al. [9], in their study of cermet coatings in rolling–sliding contact, found that the slip ratio is significant to the performance of these coatings in rolling/sliding contact. Moreover, thin coatings showed low fatigue life if the substrate surface was not blasted prior to the coating process.

In general, these studies have categorized the coatings failure as delamination and have indicated that the failure is influenced by the tribological conditions during the test. In most of the cases the failure takes place at the coating substrate interface. This can be a result of the mismatch between the coating and substrate properties, leading to stress concentrations, effects of substrate preparation before spraying and the residual stress behaviour due to the differences in thermal expansions of the coating and the substrate, etc. However, these studies give a very short account of the failure mechanisms of these coatings under the various tribological conditions, i.e. relation of coating thickness, shear stress reversal depth, lubricant film thickness and coating microstructure, etc., on the performance of these coatings. Further studies are therefore required to establish a better understanding of the fatigue wear of these coatings under low and moderate stress conditions.

2. Experimental test procedure

2.1. Test configuration

A modified four-ball machine, as shown in Fig. 1, was used to examine the RCF performance of thermally sprayed rolling elements. This machine simulates the configuration of a deep groove rolling-element ball bearing. It was used as an accelerated method for the evaluation of the RCF performance as many more stress cycles can be achieved in a fixed contact area. The coated rolling-element cone was assembled to the drive shaft via a collet, and drove the three planetary balls, which are free to rotate in a stationary cup. The drive-coated cone represents the coated inner race and the three plenary balls act as the rolling elements in the configuration of the deep groove ball bearing. The stationary cup represents the outer race of a rolling-element ball bearing in the contact model of the modified four-ball machine.

The cup assembly was loaded via a piston below the steel cup from a lever arm load to generate the required Hertz stress between the coated rolling-element and the plenary balls. Conventional cleaning methods were used to avoid contamination of the contacting surfaces in the cup assembly before the RCF tests. The tests were conducted at an ambient temperature of approximately 24 °C. The spindle speed was set to 4000 ± 5 rpm using a high-speed drive. The machine was set to stop when the vibration amplitude increased to a preset maximum value due to the failure of any rolling element in the cup assembly.

The cup assembly for the test configuration was of type II [10] having a surface hardness of 60 HRC (hardness Rockwell C). RCF tests were conducted in conventional steel ball

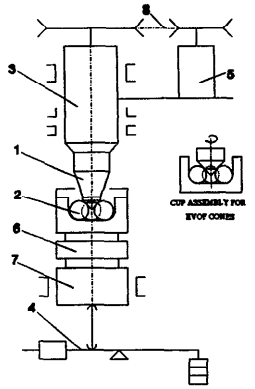

Fig. 1. Schematic of modified four-ball machine: (1) coated cone and collet; (2) planetary balls; (3) spindle; (4) loading lever; (5) driving motor; (6) heater plate; (7) loading piston; (8) belt drive.

bearing (steel plenary balls) and hybrid ceramic bearing (ceramic plenary balls) configurations. The steel lower balls were grade 10 (ISO 3290-1975) carbon chromium steel with an average surface roughness (*Ra*) of 0.02 μm and surface hardness of 64 HRC. The ceramic plenary balls were silicon nitride ceramic and manufactured by hot isostatically pressing. Ball blanks were ground and polished to a 12.7 mm diameter with an *Ra* of 0.01 μm.

2.2. Coated cone test elements

Thermally sprayed tungsten carbide cobalt (WC-12%Co) coatings produced by the high-velocity oxy-fuel (HVOF) process were deposited on the surface of the steel cones. The rolling-element cone was of 14.5 mm diameter having an apex angle of 109.2°. The substrate material was sand blasted prior to the coating process to improve the adhesive strength due to increased bonding contact area and the mechanical interlock between the substrate material and the overlay coating. The rolling elements were coated in three thicknesses by several passes of the spraying in a direction perpendicular to the cone axis. The rolling elements were ground and polished to give an average coating thickness of 150, 50 and 20 μm. The *Ra* values of the coated rolling-elements after polishing was measured to be 0.05 μm at a cutoff of 0.25 mm using a gaussian filter. The measurement direction for the average surface roughness was perpendicular to the rolling direction.

2.3. Test conditions

In order to access the performance of thermal spray coatings under various tribological conditions, three lubricants were considered during the testing programme. Lubricant A was a high viscosity paraffin hydrocarbon which has a kinematic viscosity of 200 cst at 40 °C and 40 cst at 100 °C. This lubricant was not commercially available. Lubricant B was a synthetic lubricant which has a kinematic viscosity of 12.5 cst at 40 °C and 3.2 cst at 100 °C. The test lubricant C was a mixture of distilled water and brake fluid in equal proportions by volume which were thoroughly mixed in an ultrasonic bath. This lubricant was used to access the performance of these coatings in hostile environments by making the fluid corrosive. Lubricant C was measured to have an average kinematic viscosity of 9.06 cst at room temperature of 24 °C using a Redwood viscometer. The RCF tests with the test lubricants A and B were conducted in immersed lubrication conditions. This is consistent with previous studies [8,13,14] by the authors where these lubricants did not suffer from contamination or high viscosity variations under the given test conditions. However, preliminary studies indicated that this lubrication system was inadequate for the test lubricant C, due to water evaporation owing to the flash temperature between the rolling elements and high contamination by the debris. A splash feed lubrication, shown in Fig. 2, was used to conduct RCF tests with lubricant C. This was necessary to drive the debris away from the rolling contact and to keep the lubricant viscosity constant at the inlet of the contact area. In this arrangement a micro pump having a volume flow rate range of 1170–1.2 $cm^3 h^{-1}$ was used to splash the lubricant onto the contact point through the hypodermic syringe. The contaminated lubricant was removed from the cup assembly using a gravity drain system.

The RCF tests were conducted at a load of 160 N applied to the cup assembly. The ratio (λ) of the approximate value of the elasto-hydrodynamic lubrication (EHL) film thickness [11] to the average surface roughness for the test lubricants A and B under the given test conditions was calculated to be 10 and 1.5, respectively. The EHL results for the test lubricant C are not included due to the lack of technical data such as the pressure viscosity coefficient. However, it was estimated that the λ value was less than unity under the given test conditions (for a range of pressure viscosity coefficients). This could imply that boundary lubrication exists.

Fig. 3 shows the schematic of the arrangement used to measure the total frictional torque in the modified four-ball assembly. This arrangement consists of a torque arm protruding from the base of the cup assembly which contacts a force

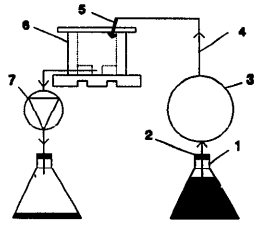

Fig. 2. Schematic of feed lubrication system: (1) flask; (2) seal; (3) micro pump; (4) flexible tubing; (5) injector syringe; (6) cup assembly; (7) flow control valve.

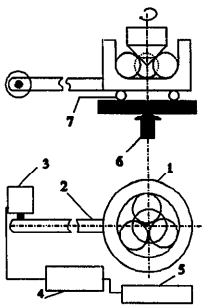

Fig. 3. Schematic of the frictional torque measurement arrangement: (1) cup assembly; (2) torque arm; (3) force transducer; (4) digital readout; (5) printer; (6) applied load; (7) rolling element thrust bearing.

transducer at the other end. The transducer is calibrated before the measurements, and the output signal is sent to a readout display and printer. The cup assembly rests on a rolling-element thrust bearing. The frictional torque measured is the sum of the frictional torque in the four-ball cup assembly and the frictional torque due to the rolling-element thrust bearing through which the load is applied to the cup assembly. Only one rolling-element cone was used for these measurements, and the frictional torque measurements were conducted under the given test conditions of contact stress and spindle speed in contact with the steel plenary balls. The average frictional torque measured for the test lubricants A, B and C was 0.043, 0.041 and 0.05 Nm, respectively. These friction values are low and indicate that the coefficient of friction between the driver and driven rolling-elements was low for the three test lubricants.

2.4. Microhardness measurements

Knoop and scratch hardness testers were used to measure the microhardness of the thermal spray coatings. These measurements were made at three different loads of 0.981, 1.962 and 2.943 N, and it was found that a load of 2.943 N gave the most statistical confidence in the microhardness results. These results indicate that the microhardness of these coatings varies from 1097 to 1390 Hv (micro Vickers hardness), with an average value of 1318 Hv. The studies of the steel substrate microhardness indicate an average value of 218 Hv at a load of 0.981 N. Studies were also made to investigate any difference in the values of microhardness on the surface and the coating cross-section, due to the lamellar structure and anisotropy. These studies were carried out on a flat steel substrate to avoid any error in the results due to surface curvature of the rolling elements. A 200 μm coating was prepared on a flat substrate for this analysis and measurements were made at the above-mentioned loads. The results indicate that the average surface microhardness of these coatings was approximately the same as the through thickness microhardness at the 2.943 N load. During these measurements it was found that the coating can crack at certain locations at low loads of 0.981 N, whereas at other sections the coating does not crack even at a higher load of 2.943 N. This behaviour was evident on the surface as well as through thickness measurements. A typical result is shown in Fig. 4, in which the crack propagated at a load of 0.981 N. There was no definite trend in this anisotropic behaviour of the coating and it is appreciated that the fracture toughness of the lamellar structure of the coating is different within the microstructure.

The weakness in the coating microstructure was also seen in a simple compression test in the four-ball machine. The coated rolling-element cone was loaded at a Hertz contact stress of approximately 6 GPa in a clean, dry contact with the stationary plenary steel balls of the four-ball machine. The load was removed and it was observed that the surface of the rolling-element cone peeled as shown in Fig. 5. The coating particles adhered to the ball surface. This shows that the deformation resistance of the coating substrate combination was low. Moreover, the cohesive strength between the lamellae is low and the coating is prone to peeling in the absence of shear force. This can indicate the weakness and brittleness of the coating microstructure. Cracks can also be seen on the edge of the contact area due to the tensile stress.

Fig. 4. Microhardness indentation (load 100 p).

Fig. 5. Coating surface.

2.5. Coating microstructure

Fig. 6 shows a typical microstructure of the coating cross-section in SEM. The secondary electron image (SEI) is shown in Fig. 6(a), whereas Fig. 6(b) shows the back-scattered electron image (BEI). The comparison of the two images shows that the amount of retained WC particles is high which is typical of the HVOF process. The size of retained WC particles varies from 1 to 5 μm. Secondary-phase particles are not common in the microstructure. However, there are numerous pores and cracks evident in the coating microstructure. The average coating porosity can be approximated as 1%. It should be appreciated that it is not only the magnitude of porosity, etc., but also the shape of microcracks which can lead to stress concentrations and thus affect the RCF life. X-ray diffraction analysis of the microstructure confirmed that the amount of retained WC particles was high with small quantities of W_2C particles. This is consistent with the work done by Harvey et al. [12], and is indicative of the high wear resistance of the coatings.

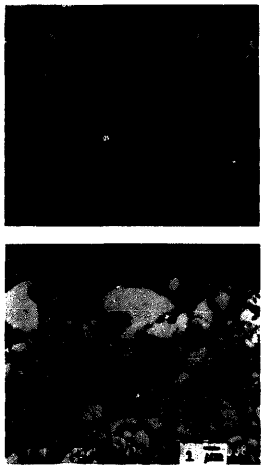

Fig. 6. Coating microstructure.

3. Experimental test results and surface observations

3.1. Test results

Table 1 shows the RCF test results for the HVOF-coated rolling-element cones under the various tribological conditions of testing. Results are presented in terms of the test configuration, coating thickness, Hertz contact stress, location and magnitude of orthogonal shear stress and the time to failure. The magnitude and location of stresses shown in Table 1 represent the case of uncoated rolling-elements. These results are included to give an indication of the stress fields within the rolling elements under the given test conditions, since the case of coating substrate combination cannot be readily applied in the Hertzian contact analysis. One approach could be to use the approximate solution using computer modelling, as indicated in the previous studies by the authors [13]. However, the coating porosity and anisotropy need to be considered, which can make these models complex and expensive to solve. The RCF test results give an appreciation of the performance of the coated elements and are not intended to be used as a basis for statistical fatigue life prediction. The test results indicate that the coating thickness and the lubricant type can have significant effects on the RCF performance of these coatings.

3.2. Surface observations

Fig. 7 shows the surface observations of a 150 μm-thick coated rolling-element tested in lubricant A in contact with the steel lower balls. Fig. 7(a) shows the BEI of the overall area of the failed coating. It can be seen that the coating failed from within the microstructure as indicated by the bright (high atomic number contrast) image. The presence of the coating was confirmed by electron probe microscope analysis (EPMA) at the failed coating section. The SEM image of the failed coating at a higher magnification at an inclined angle is shown in Fig. 7(b). This figure also shows the coating debris which are about to delaminate from the wear track. Fig. 7(c) shows the failed coating at an inclined angle at a higher magnification. The coating failure was parallel to the surface of the rolling element. This type of delamination failure from within the coating microstructure was seen in all the tests conducted with 150 and 50 μm-thick coatings.

Fig. 8 shows the SEM observations of a 20 μm-thick coating tested in lubricant B with steel lower balls. The test was suspended after 16 million stress cycles. Fig. 8(a) shows the surface of the rolling element cone in BEI. It can be seen that the coating is intact with the substrate, with no microcracks

Table 1
RCF test results

Test	Average coating thickness (μm)	Lubricant type	Planetary balls	[a]Peak compressive stress (P_o) (GPa)	[a]Orthogonal shear stress ($0.21P_o$) (GPa)	[a]Contact width (a) (major axis) (mm)	[a]Depth of orthogonal shear ($0.3a$) (μm)	Time to failure (min)
T1	150	A	Steel	1.7	0.36	0.133	40	288
T2	150	B	Steel	1.7	0.36	0.133	40	2118
T3	50	A	Steel	1.7	0.36	0.133	40	3420
T4	50	B	Steel	1.7	0.36	0.133	40	1740
T5	50	C	Steel	1.7	0.36	0.133	40	162
T6	50	C	Ceramic	1.9	0.40	0.125	37	18
T7	20	A	Steel	1.7	0.36	0.133	40	7620
T8	20	B	Steel	1.7	0.36	0.13	40	912
T9	20	C	Steel	1.7	0.36	0.133	40	640
T10	20	C	Ceramic	1.9	0.40	0.125	37	339

[a] Uncoated case.

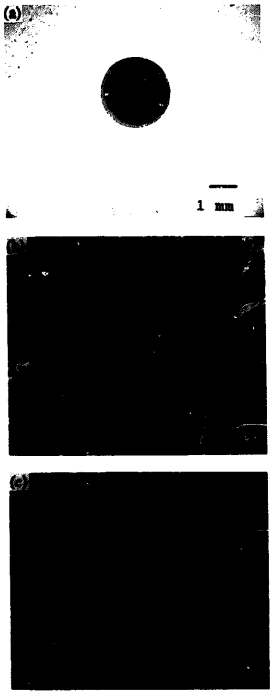

Fig. 7. SEM observations of 150 μm thick coatings in lubricant A.

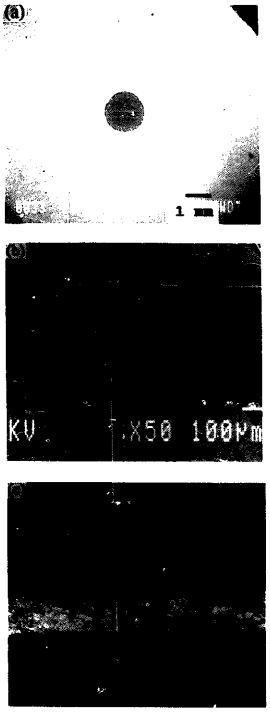

Fig. 8. SEM observations of 20 μm thick coating in lubricant B.

visible on the wear track. Fig. 8(b) shows an SEM observation of the wear track, and small pits can be seen on the surface of the wear track. Fig. 8(c) shows the cross-section of the wear track. Cracks and pits can be seen on the surface of the wear track, some of which could have been caused during the sectioning and polishing of the coating. However, it is interesting to note that no delamination cracks are visible underneath the wear track. Fig. 9 shows a typical talysurf observation of the wear track of this rolling element after the RCF test. The figure indicates that there may be some coating deformation at the edge of the wear, which is consistent with the previous studies by the authors [14].

Fig. 10 shows the BEI of the surface of the rolling element cone tested in lubricant C in contact with the ceramic lower balls. Fig. 10(a) shows the BEI of the overall view of the wear track. It can be seen that the coating is still intact with the substrate; however, an appreciable amount of surface wear can be seen on the wear track. Fig. 10(b) shows the wear track pit at a higher magnification in the BEI. The presence of coating material at the bright portions was confirmed by EPMA analysis. It can be seen that the coating failure is from the substrate material. This behaviour is more evident in Fig. 10(c) which shows the cross-section of the wear track. This figure shows plastic deformation and cracks in the substrate material.

Surface observations of the plenary balls after the RCF tests indicate that WC debris were present on the surface of the rolling-element balls. Fig. 11 shows a typical result which shows debris (BEI) on the surface of the plenary balls tested in lubricant C. This behaviour was commonly seen in the tests conducted with lubricant C. However, the occurrence of

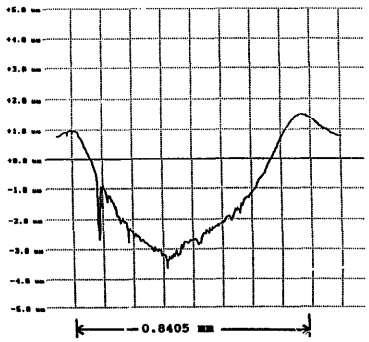

Fig. 9. Talysurf analysis of the wear track of 20 μm coating.

embedded WC debris particles on the lower balls was rare for tests conducted in lubricants A and B.

Fig. 12 shows SEM surface observations of a failed coating debris particle for a 150 μm-thick coated rolling-element tested in lubricant B. Fig. 12(a) shows the top surface of the delaminated particle. Fig. 12(b) shows an SEM representation of the failed surface of the debris particle. Fig. 12(c) shows the debris particle edge at an inclined angle and gives an appreciation of its thickness. The debris particle size can be approximated as 800×500×70 μm. However, this debris size was rare in the test lubricants. In general, the debris for 150 and 50 μm-thick coatings were smaller in size and approximately half of the dimensions of the particle shown in Fig. 12. However, the debris for the tests conducted with 20 μm thick coatings were much smaller in size. It is possible that the small size of debris was due to the rolling of debris between the rolling elements after the coating failure.

4. Discussion

The RCF test results indicate that the coatings performed better with the high viscosity lubricant (A). Moreover, thinner coatings (20 μm) showed a longer RCF life than the thicker coatings (50 and 150 μm). However, the trend was not consistent for lubricant B. The tests with the ceramic lower balls (lubricant C) showed reduced RCF life in comparison with the tests conducted with steel lower balls. It can be a result of higher stresses due to higher modulus of elasticity of the ceramic balls. The surface observations of the failed coated rolling-elements indicate that two possible wear mechanisms are operational in the failure of these coatings, i.e. delamination of the coating underneath the wear track and surface wear due to the asperity contact. The friction measurements indicate that there was marginal differences in the magnitude of the frictional torque for the three lubricants.

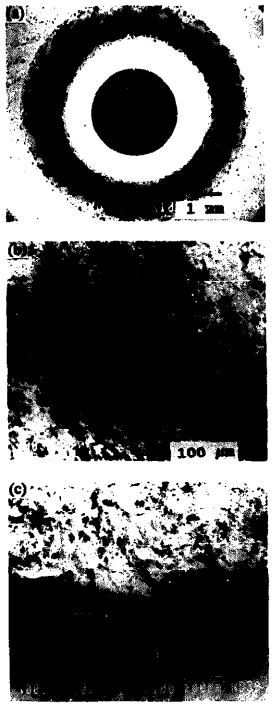

Fig. 10. SEM observations of 20 μm thick coating in lubricant C.

Hence it can be established that the frictional forces did not significantly influence the coating failures for the three lubricants.

Delamination behaviour [Fig. 7(b)] was seen in all the cases for 50 and 150 μm-thick coatings. The depth of failure in these coatings can be approximated as 40 μm [Fig. 7(c)]. Most of these failures were parallel to the surface [Fig. 7(b)]. This is mainly due to crack propagation in the coating microstructure parallel to the surface. This may have been caused by orthogonal shear-stress reversal underneath the wear track. This is consistent with previous studies by the authors [13]. Although the depth of orthogonal shear stress reversal for coated rolling-elements will vary from the values shown in Table 1, there is good agreement between the depth of failure and indicated depth of stress reversal. Moreover, most of the debris in the test lubricants had the thickness of

Fig. 11. Debris on the planetary balls (BEI).

approximately 30 μm, which is close to the depth of failure. However, in rare cases, as indicated in Fig. 12, these debris can be much thicker, which can be related to the approximate depth of maximum shear stress. The specific nature of thermal spraying results in layers of the coating material parallel to the surface. This microstructure contain pores and microcracks not only within the individual layers, but also between the layers. Orthogonal shear-stress reversal causes stress concentration in these pores and cracks. This results in crack propagation parallel to the surface at the depth of orthogonal shear stress reversal. These cracks emerge on the surface at the edge of the wear track due to tensile stress at the edge of the contact area. This results in a delamination of the coating parallel to the surface of the wear track. The reason that 20 μm coatings did not fail in delamination within the coating microstructure can be explained by the shift of the depth of the shear-stress reversal into the substrate material. Hence the substrate material is critical to the RCF performance. This can be seen in Fig. 10(c), in which cracks are visible in the substrate material. However, thinner coatings can suffer from stress concentration at the interface, due to the difference in the modulus of elasticity of the coating and the substrate material. Since coating delamination at the interface was not observed for the 20 μm thick coatings it was appreciated that the mechanical interlock at the interface and the compressive residual stresses due to the difference in coefficient of thermal expansion of the coating and substrate material resisted this failure mechanism.

Surface wear of the coating due to the asperity contact can be explained on the basis of the weak interlamellar strength of the coating, as was seen by the generation of the cracks during the hardness measurements and the peeling behaviour of the coating (Figs. 4 and 5). It is possible that mixed and boundary lubrication conditions during the tests conducted with lubricants B and C resulted in adhesion of asperities. The adhesion weld shear within the weak lamella structure of the coating resulted in small pits on the surface of the wear track. This is also evident from the presence of WC debris on the surface of the plenary balls. The fact that in rare cases some WC debris were present on the surface of the plenary balls for the test lubricant A, where the fluid film thickness

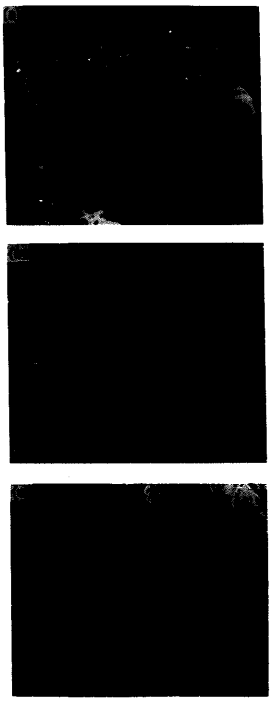

Fig. 12. SEM observations of debris particle in lubricant B.

should prevent asperity contact, is thought to occur during the start of the test, when the fluid film was not fully developed. However, there is also a possibility that these debris were not a result a of adhesion, but debris produced during the RCF test by other wear mechanisms, or delaminations were embedded on the surface of the plenary balls due to the higher hardness of the coating debris, by rolling between the cup and the plenary balls.

The talysurf analysis of the wear track indicates plastic deformation may be present at the edge of the wear track. This could be due to the ductile nature of the coating and low hardness of the substrate material. However, no microscopic studies were done to examine this behaviour. This behaviour was more prominent when the coatings were tested at higher stresses, where large plastic deformations were observed at the edge of the wear track, as indicated in previous studies

by the authors [14]. In general, it is seen that the substrate hardness to support the coating, coating thickness to alter the depth of orthogonal shear stress reversal and the lamellar coating microstructure are important to the RCF performance of the coatings. The surface wear at the wear track indicates that the surface roughness and lubrication film, which can alter the asperity contact behaviour, are critical to the performance of these coatings. Studies were also made to investigate any oxidation effect of test lubricant C, but no such evidence was found on the surface of the wear track. This can be due to the high corrosive resistance of WC-Co coatings.

5. Conclusions

(1) Thinner coatings performed better, especially with a high viscosity lubricant, and the coatings failure was a combination of surface wear and subsurface delamination.
(2) The coating wear is dependent upon the coating thickness and tribological conditions during the test, which can be attributed to the effects of film thickness and the variations caused in the location of the shear stresses in the coated rolling-elements for coatings with different thicknesses.
(3) Thick coatings delaminate from within the coating microstructure parallel to the surface, and the delaminated coating debris varied in thickness.

Acknowledgements

The authors of this paper acknowledge the support of Professor Shogo Tobe of the Ashikaga Institute of Technology for his help in the preparation of the test samples. The authors also acknowledge the financial support of the ORS (Overseas Research Scholarship) for partly funding the project.

References

[1] P. Vuoristo, K. Niemi, A. Makela and T. Mantyla, *Conf. Proc., National Thermal Spray Conf., Anaheim, CA, USA, 1993*, pp. 635–641.
[2] M.K. Kesharan and K.T. Kembaiyan, *Conf. Proc., National Thermal Spray Conf., Anaheim, CA, USA, 1993*, pp. 635–641.
[3] A. Ohmori, *Conf. Proc., Int. Thermal Spray Conf., Kobe, Japan, May, 1995.*
[4] S. Tobe, S. Kodama and K. Sekiguchi, *Conf. Proc., Surface Engineering Int. Conf., Tokyo, Japan. 1988*, pp. 35–44.
[5] S. Tobe, S. Kodama and H. Misawa, *Conf. Proc., Thermal Spray Research and Applications, 1991*, pp. 171–178.
[6] A. Makela, P. Vuoristo, M. Lahdensuo, K. Niemi and T. Mantyla, *Conf. Proc., Thermal Spray Industrial Applications, 1994*, pp. 759–764.
[7] P. Sahoo, *Powder Metall. Int.*, 25 (1993) 73–78.
[8] M. Hadfield, R. Ahmed and S. Tobe, *Conf. Proc., Int. Thermal Spray Conf., Kobe, Japan, May, 1995*, pp. 1097–1102.
[9] M. Yoshida, K. Tani, A. Nakahira, A. Nakajima and T. Mawatari, *Conf. Proc., Int. Thermal Spray Conf., Kobe, Japan, May, 1995*, pp. 663–668.
[10] R. Tourret and E.P. Wright, *Int. Symp., I. Petroleum, October, 1976*, Heyden and Son, London, 1977.
[11] B.O. Jacobson, *Rheology and Elastohydrodynamic Lubrication*, Baker and Taylor, 1991.
[12] M. Harvey, A. Sturgeon, F. Blunt and S. Dunkerton, *Conf. Proc., Int. Thermal Spray Conf., Kobe, Japan, May, 1995*, pp. 471–476.
[13] R. Ahmed and M. Hadfield, *Surf. Coat. Technol.*, 82 (1996) 176–186.
[14] R. Ahmed and M. Hadfield, *Conf. Proc., 4th Int. Conf. on Advances in Surface Engineering, Newcastle, UK, 1996.*